Supplementary Information

Fabrication of 2D/2D $Bi_2MoO_6/S_x@g-C_3N_{(4-y)}$ type-II heterojunction photocatalyst for enhanced visible-light-mediated degradation of tetracycline in wastewater

Soorya K K [a], Adarsh Singh [a], Suneel Kumar Srivastava [b δ], Animesh Bhattacharya [c], Amit Bhatnagar [d], Ashok Kumar Gupta [a *]*

[a] Environmental Engineering Division, Department of Civil Engineering,

Indian Institute of Technology Kharagpur, Kharagpur 721302, India

[b] Department of Chemistry,

Indian Institute of Technology Kharagpur, Kharagpur 721302, India

[c] School of Environmental Science and Engineering,

Indian Institute of Technology Kharagpur, Kharagpur 721302, India

[d] Department of Separation Science, LUT School of Engineering Science,

LUT University, Sammonkatu 12, Mikkeli FI-50130, Finland

* Corresponding author.
E-mail address: agupta@civil.iitkgp.ac.in (A. K. Gupta).
E-mail address: suneelchemkgp@gmail.com ([δ]S. K. Srivastava, former faculty, IIT Kharagpur).

Section S1 Thermogravimetric analysis (TGA) of BS_xN_y (II)

About 1.47% weight loss is observed on heating BS_xN_y (II) in the temperature range of 30°-810 °C. Reportedly, pristine Bi_2MoO_6 exhibited stability up to 800°C with minor weight loss.[1] In contrast, rapid decomposition is observed in the thermogram of g-C_3N_4 at around 600°C.[2] It is noted that the weight loss profile in the thermogram of BS_xN_y (II) can be divided into three stages. The first step (25-200°C) comprises the weight loss attributed to the expulsion of adsorbed water from the BS_xN_y (II). Subsequent weight loss in TGA occurs in the range of 200 °C - 500°C due to the initiation of S loss from S_x@g-$C_3N_{(4-y)}$.[3] The significant weight loss in the final step at around 600°C could possibly be due to the decomposition of S_x@g-$C_3N_{(4-y)}$ in the heterojunction.

Section S2 Synthesis of pristine g-C_3N_4

Pristine g-C_3N_4 was synthesized using a previously reported method.[4] In a typical synthesis procedure, 10 g of melamine was calcined in a muffle furnace at a temperature of 550°C for 4 h with a heating rate of 20°C/min. The resulting yellow product was then crushed into fine powder after cooling to ambient temperature.

Section S3 Effect of cations on photocatalytic degradation efficiency of tetracycline (TCL)

The Fe^{3+} ions in the reaction mixture showcased an inhibitory effect on photocatalytic degradation of TCL, decreasing degradation efficiency to 84.7%. This can be due to the conversion of Fe^{3+} to $Fe(OH)_2^+$, which tend to absorb a part of incident photons.[5] On the contrary, the complex formed due to the interaction between Ca^{2+} and TCL reportedly increases light absorption, as reflected by the negligible decrease in degradation efficiency.[6,7]

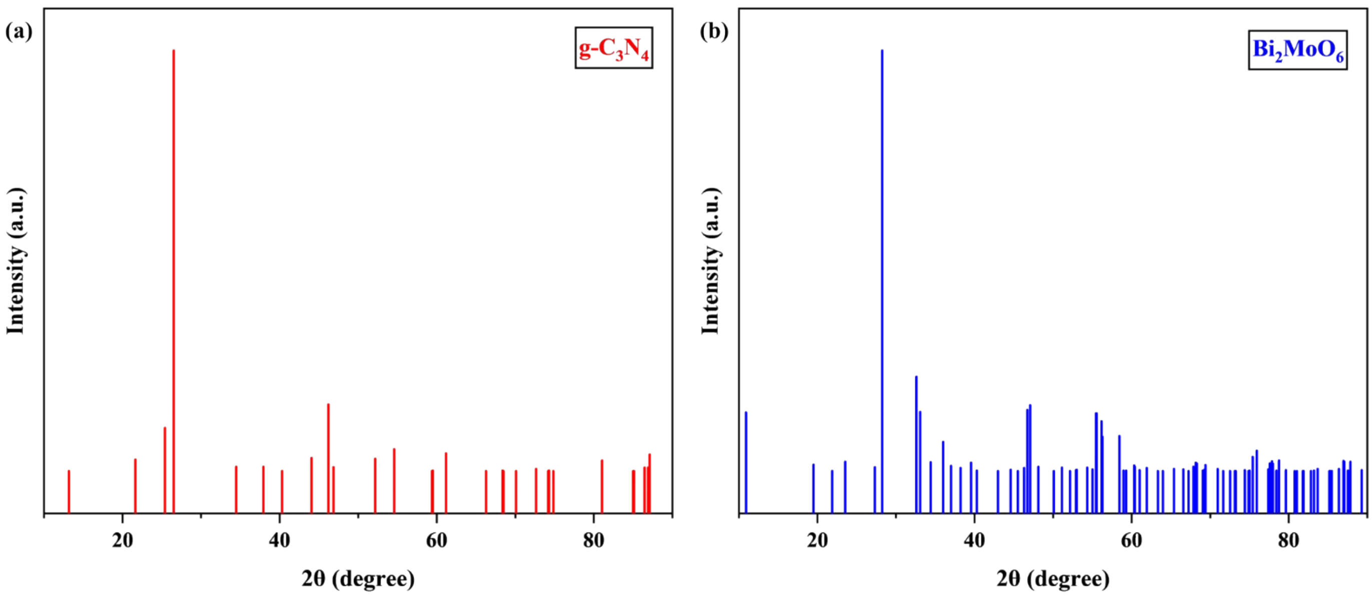

Fig. S1 XRD pattern of (a) $g\text{-}C_3N_4$ (JCPDS card no. - 01-087-1526), (b) Bi_2MoO_6 (JCPDS card no. - 01-076-2388) from standard atlas card for crystal planes.

ISO 25178			
Height Parameters			
Sq	1.02	nm	*Root mean square height*
Ssk	1.35		*Skewness*
Sku	16.1		*Kurtosis*
Sp	18.3	nm	*Maximum peak height*
Sv	4.01	nm	*Maximum pit height*
Sz	22.3	nm	*Maximum height*
Sa	0.774	nm	*Arithmetic mean height*

Fig. S2 Height parameters of BS_xN_y (II) composite.

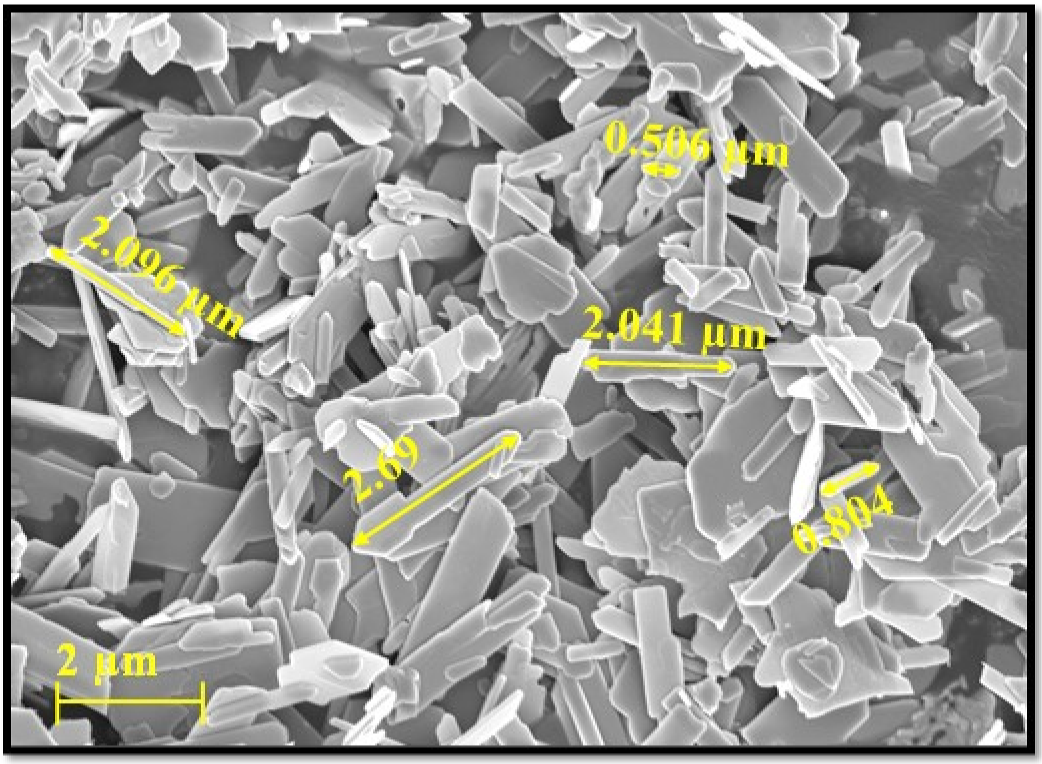

Fig. S3 FEG-SEM images depicting particle size of Bi_2MoO_6.

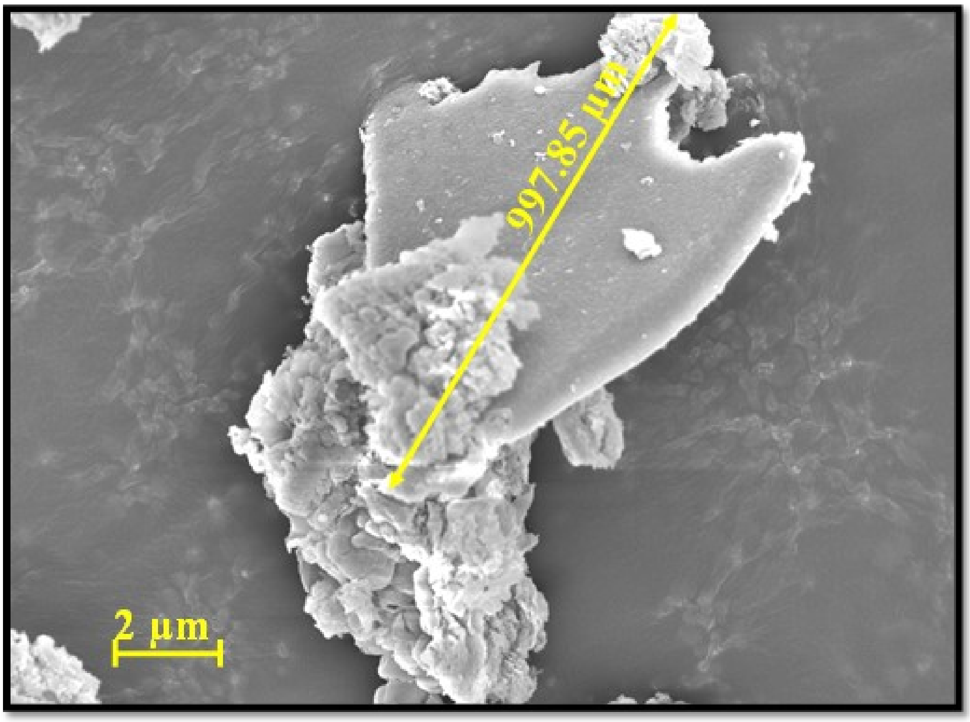

Fig. S4 FEG-SEM images depicting particle size of $S_x@g\text{-}C_3N_{(4\text{-}y)}$.

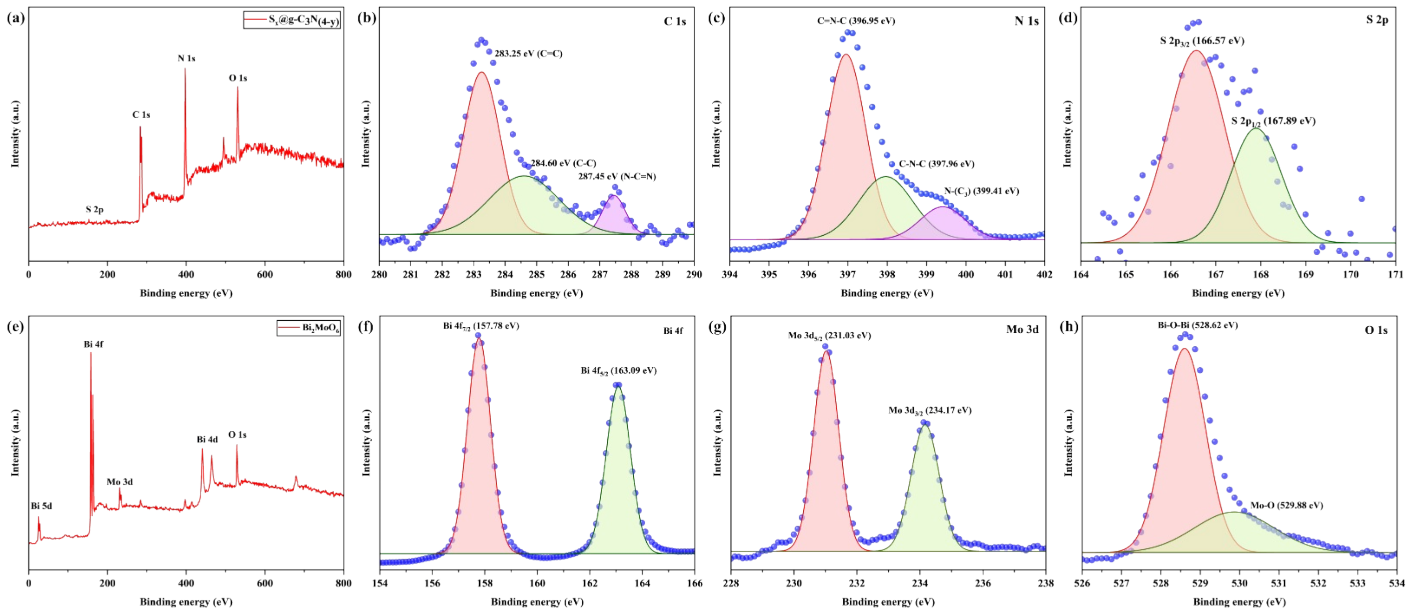

Fig. S5 (a) XPS survey scan of $S_x@g\text{-}C_3N_{(4\text{-}y)}$, high-resolution spectra of (b) C 1s, (c) N 1s, (d) S 2p, (e) XPS survey scan of Bi_2MoO_6, high-resolution spectra of (f) Bi 4f, (g) Mo 3d, and (h) O 1s.

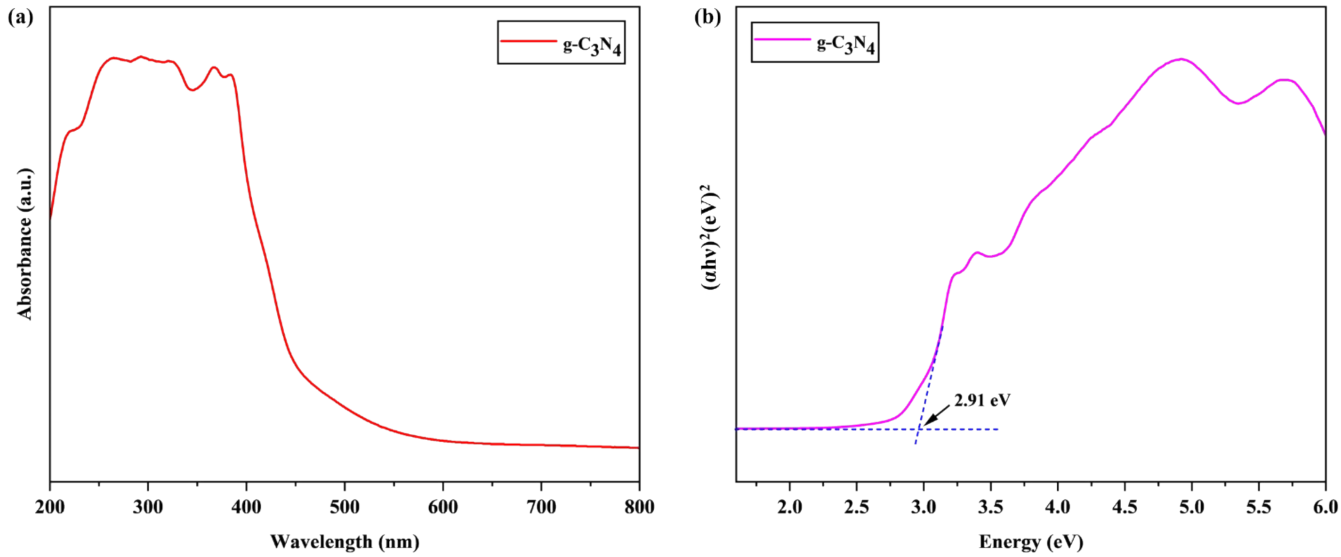

Fig. S6 (a) UV-Vis DRS spectra, and (b) Tauc plot of $g\text{-}C_3N_4$ synthesized using melamine as briefed in section S2.

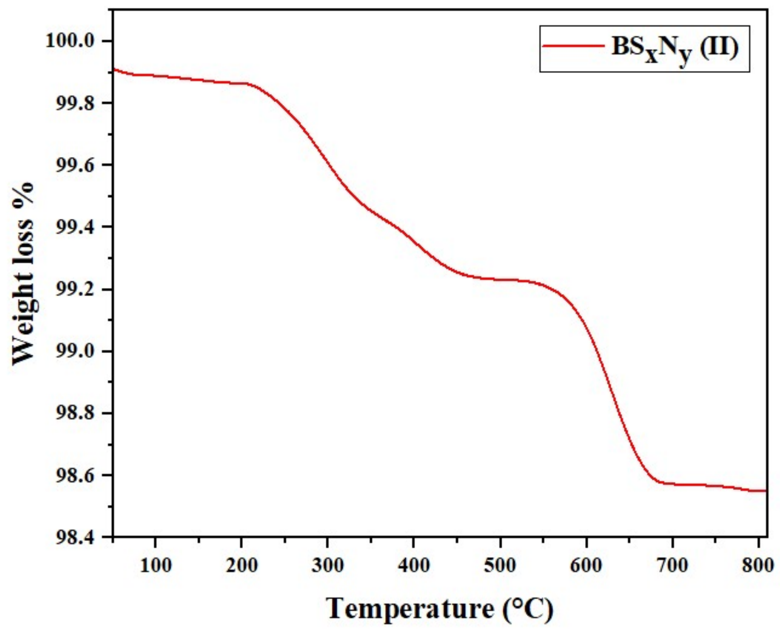

Fig. S7 Thermogravimetric analysis (TGA) curve of BS_xN_y (II) composite.

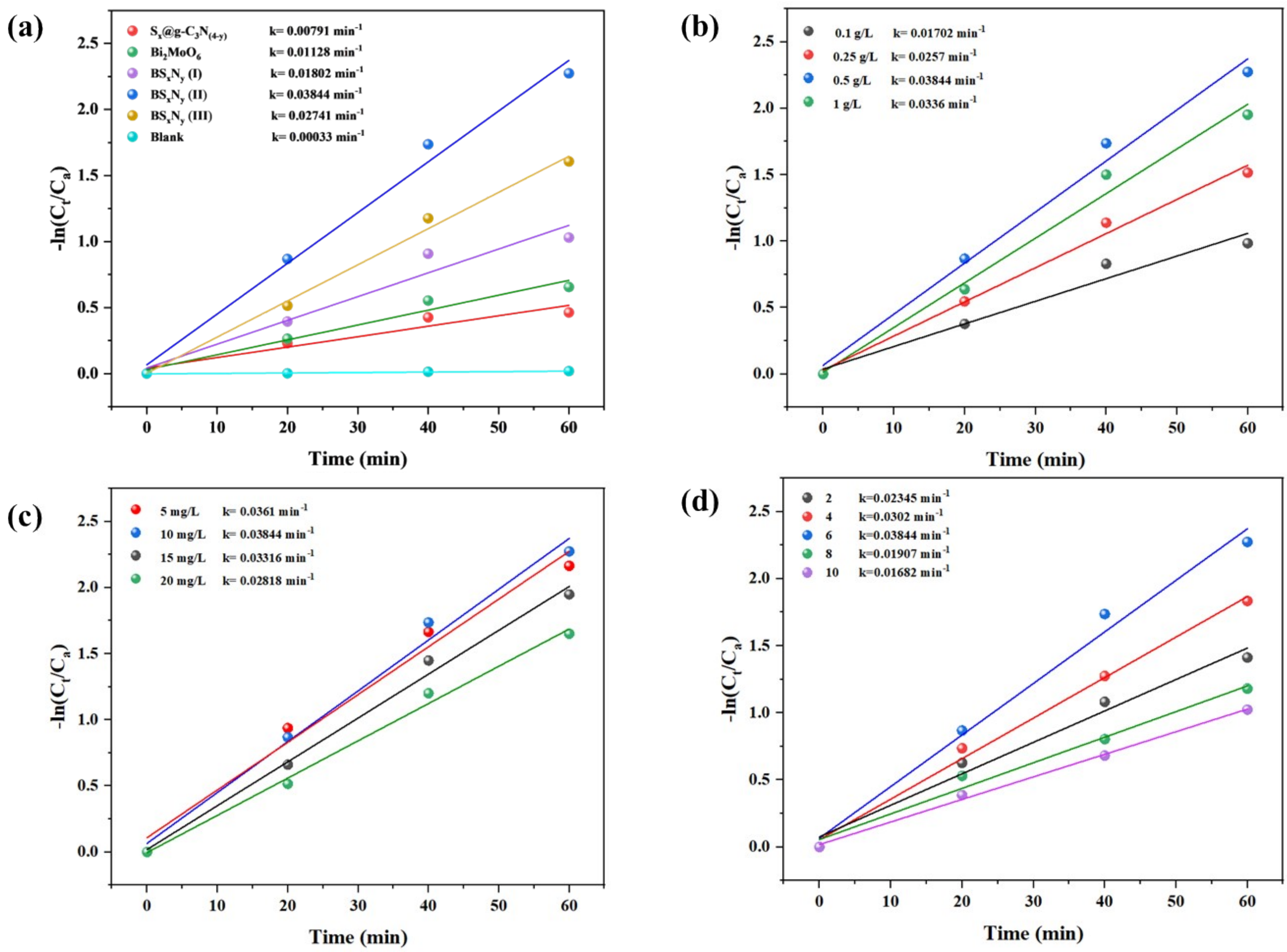

Fig. S8 Pseudo-first-order degradation kinetics plots for tetracycline (TCL) degradation using BS_xN_y.

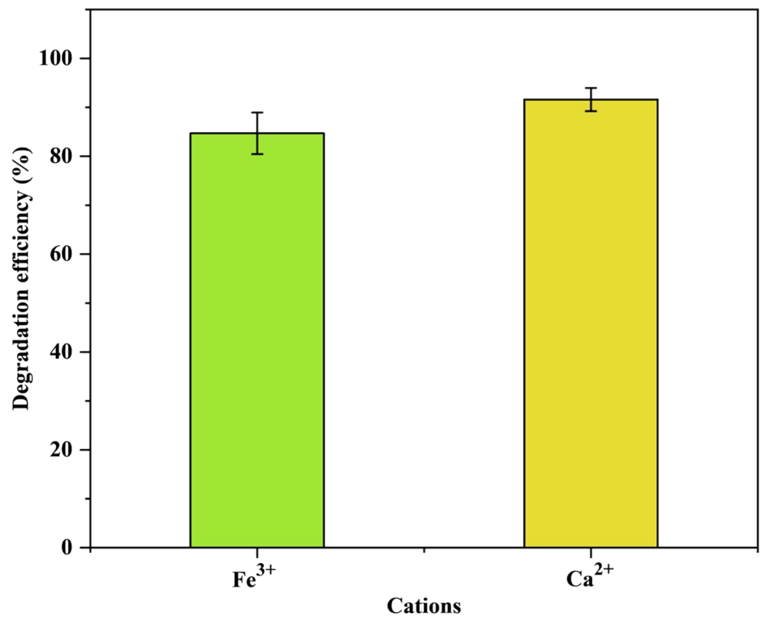

Fig. S9 Influence of cations on the photocatalytic degradation of TCL.

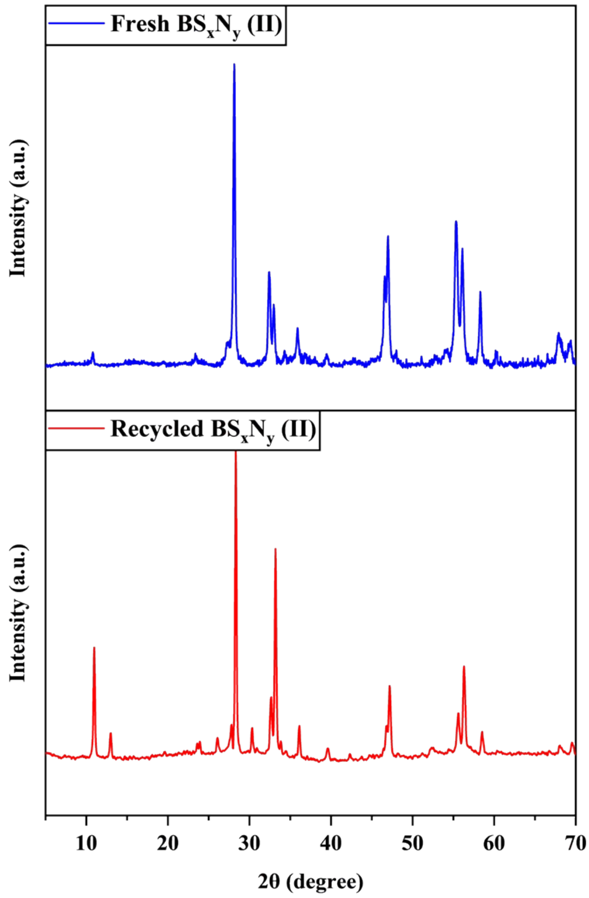

Fig. S10 XRD pattern of (a) fresh BS_xN_y (II), and (b) recycled BS_xN_y (II).

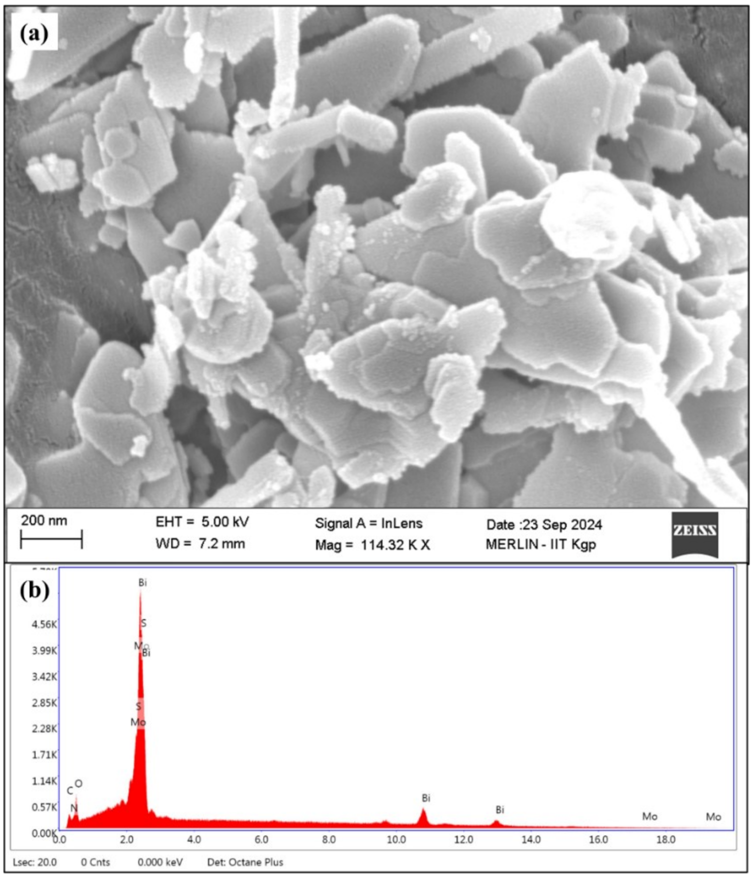

Fig. S11 (a) FEG-SEM image, and (b) EDS spectra of BS_xN_y (II) after reusability study.

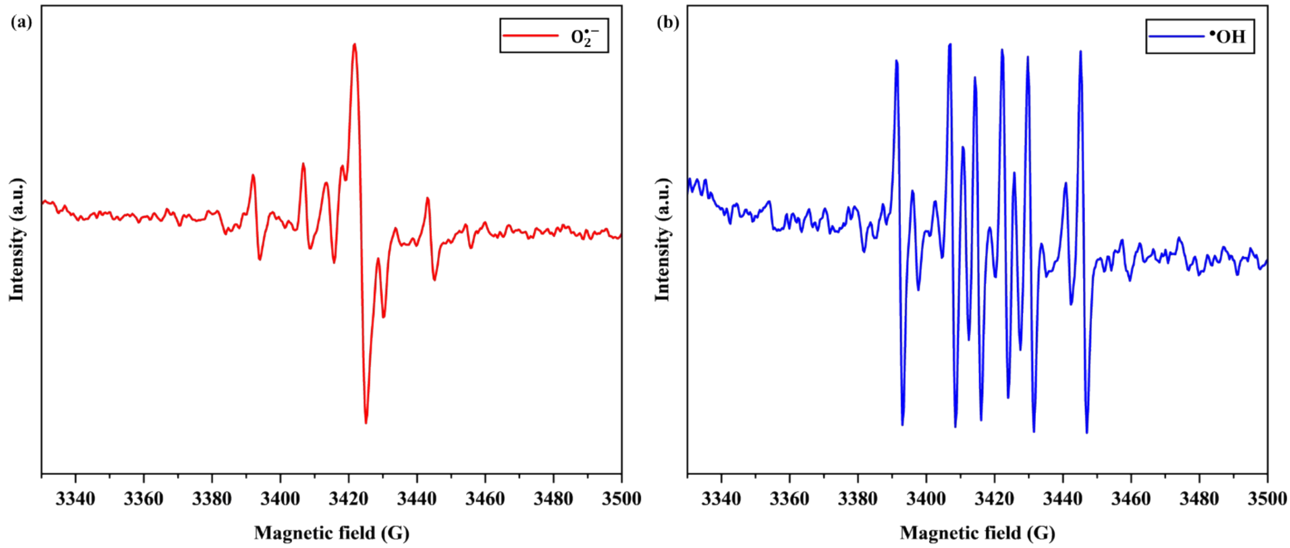

Fig. S12 EPR spectra of (a) DMPO-$O_2^{\bullet -}$, and (b) DMPO-•OH radicals.

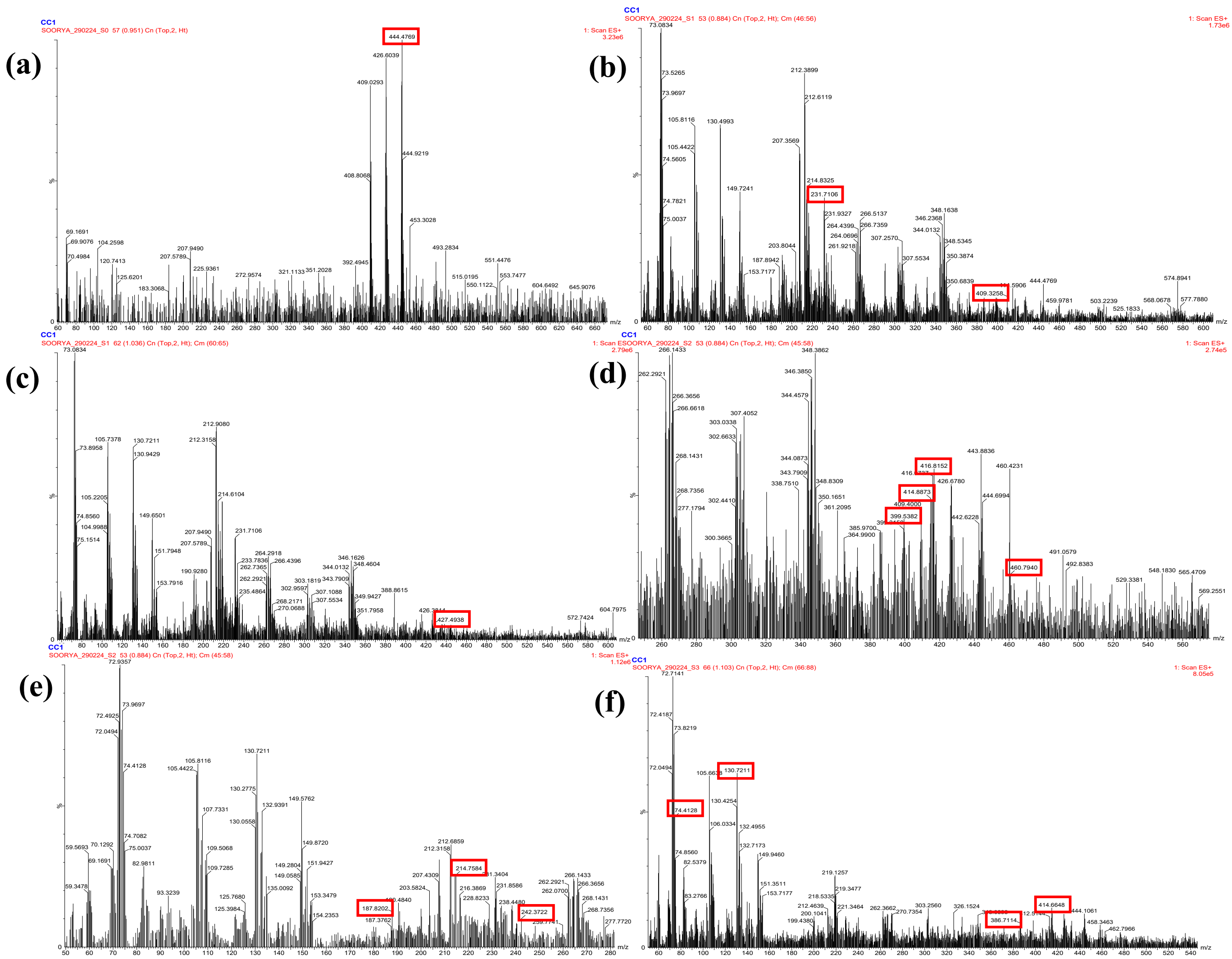

Fig. S13 LC-MS chromatograph displaying identified transformation products (TPs) of TCL.

Table S1 Detailed information on the chemicals used in this work.

S. No.	Chemical	Source
1	Ammonium molybdate tetrahydrate ($(NH_4)_6Mo_7O_{24}.4H_2O$)	Merck, India
2	Bismuth nitrate pentahydrate ($Bi(NO_3)_3\cdot5H_2O$)	Merck, India
3	Thiourea (CH_4N_2S)	Merck, India
4	Ethylene glycol ($C_2H_6O_2$)	Merck, India
5	Ethanol (C_2H_5OH)	Merck, India
6	Tetracycline ($C_{22}H_{24}N_2O_8$)	Sigma-Aldrich

Table S2 Instruments used in the characterization and analysis.

S. No.	Characterization and analysis technique	Company	Purpose
1	X-ray diffraction (XRD) analysis	D2 Phaser, Bruker, USA	To analyze the crystal structure
2	Fourier-transform infrared spectroscopy (FTIR)	Bruker Alpha II	To identify functional groups and chemical composition
3	Field emission gun scanning electron microscopy (FEG-SEM) Energy dispersive X-ray spectroscopy (EDS)	Zeiss Merlin Gemini II, Germany	To observe the surface morphology and elemental composition
4	Atomic force microscopy (AFM)	Agilent 5500 Atomic Force Microscope	To characterize surface topography
5	X-ray Photoelectron Spectroscopy (XPS)	PHI 5000 VersaProbe III, ULVAC PHI Inc., USA	To analyze surface chemistry
6	UV-Vis diffuse reflectance spectroscopy	Cary 5000 UV-Vis-NIR spectrophotometer	To study the optical properties
7	Inductively coupled plasma optical emission spectroscopy (ICP-OES)	iCAP PRO, Thermo Scientific, USA	To determine metal leaching
8	Thermo-gravimetric and Differential Thermal Analysis (TGA-DTA)	Perkin Elmer Pyris Diamond	To investigate thermal stability and decomposition kinetics
9	Liquid chromatography-mass spectrometry (LC-MS)	Quattro microTM API, Waters, USA	To analyze transformation products
10	Spectrophotometer	Cary 60 UV-Vis Spectrophotometer	To measure aliquot concentration
11	CHNS-O analyzer	Euro EA CHNSO Analyzer	To evaluate the chemical composition
12	High-resolution transmission electron microscopy (HRTEM)	JEOL (JEM-ARM300F2) (Double Aberration-corrected 300 kV HRTEM)	To perform high-resolution imaging and elemental mapping of the catalyst.
13	Pulsed Electron paramagnetic resonance (EPR) Spectrometer (X-band)	Bruker (ELEXSYS 580)	To identify active species facilitating photocatalytic degradation.

Table S3 CHNS-O analysis of $S@g-C_3N_4$ and $S_x@g-C_3N_{(4-y)}$.

Material	C (wt. %)	N (wt. %)	H (wt.%)	S, O (wt.%)
$S@g-C_3N_4$	31.65	61.32	1.76	5.27
$S_x@g-C_3N_{(4-y)}$	31.72	59.83	1.42	7.02

Table S4 Binding energy peaks from XPS spectra (Fig. S4), and associated assignments from literature.

S. No.	Photocatalyst	Element	Binding energy (eV)	Assignments		References
1	Bi_2MoO_6	Bi 4f	163.09 eV	Bi $4f_{5/2}$	Bi^{3+}	8,9
			157.78 eV	Bi $4f_{7/2}$		
		O 1s	528.62 eV	Bi-O-Bi		10,11
			529.88 eV	Mo-O		
		Mo 3d	231.03 eV	Mo $3d_{5/2}$		12
			234.17 eV	Mo $3d_{3/2}$		
2	$S_x@g-C_3N_{(4-y)}$	C 1s	283.15 eV	C=C		13–15
			284.60 eV	C-C		
			287.45 eV	N–C=N		
		N 1s	396.95 eV	C-N		16–18
			397.96 eV	C-N=C		
			399.41 eV	N-(C_3)		
		S 2p	166.57 eV	S $2p_{3/2}$		19
			167.89 eV	S $2p_{1/2}$		

Table S5 Pseudo-first order rate constants for photocatalytic degradation of TCL in different reaction conditions.

Parameters	Reaction Conditions	k (min^{-1})	R^2
Photocatalysts	$S_x@g-C_3N_{(4-y)}$	0.00791	0.92599
	Bi_2MoO_6	0.01128	0.96713
	BS_xN_y (I)	0.01802	0.95375
	BS_xN_y (II)	0.03844	0.98899
	BS_xN_y (III)	0.02741	0.99402
BS_xN_y (II) dose (g/L)	0.1 g/L	0.01702	0.96792
	0.25 g/L	0.0257	0.99208
	0.5 g/L	0.03844	0.98899
	1 g/L	0.0336	0.98736
Initial TCL concentration (mg/L)	5 mg/L	0.0361	0.98194
	10 mg/L	0.03844	0.98899

	15 mg/L	0.03316	0.9932
	20 mg/L	0.02818	0.99132
pH	2	0.02345	0.98028
	4	0.0302	0.99451
	6	0.03844	0.98899
	8	0.01907	0.98341
	10	0.01682	0.99735

Table S6 Comparison of photocatalytic performance of Bi_2MoO_6 and $g\text{-}C_3N_4$ based catalysts for TCL degradation.

Photocatalyst	**Light source**	**Initial TCL concentration**	**Catalyst dosage**	**pH**	**Degradation efficiency**	**Mechanism**	**References**
10%-$CuBi_2O_4$/ Bi_2MoO_6	300 W xenon lamp	20 mg/L	0.3 g/L	-	72.8% (60 min)	Type II	20
SnS_2/ Bi_2MoO_{6-x}	300 W xenon lamp	20 mg/L	0.3 g/L	6	89% (90 min)	Z-Scheme	21
15% $g\text{-}C_3N_4$/ Bi_2MoO_6/ Bi_2WO_6	500 W tungsten halogen lamp	30 mg/L	0.25 g/L	-	98% (90 min)	Z-Scheme	22
Bi_2MoO_6/ $g\text{-}C_3N_4$	300 W xenon lamp	10 mg/L	1 g/L	5	97.5% (120 min)	Type II	23
BiOCl/ Bi_2MoO_6	350 W xenon lamp	10 mg/L	1 g/L	7	97.23% (100 min)	Type II	24
ZrO_2 modified S-doped $g\text{-}C_3N_4$	300 W xenon lamp	40 mg/L	0.6 g/L	8.5	72.2% (150 min)	Type II	25
N defect engineered $g\text{-}C_3N_4$	50 W LED lamp	20 mg/L	1 g/L	4.7	78% (120 min)	-	26
BS_xN_y (II)	**50 W LED lamp**	**10 mg/L**	**0.5 g/L**	**6**	**92.4% (60 min)**	**Type II**	**This study**

Table S7 Water quality parameters for different water matrices.

Parameters	**DI water**	**Tap water**	**Municipal wastewater**
pH	6.7±0.2	7.1±0.3	6.9±0.2
Turbidity (NTU)	-	2.1±0.8	52.8±3.1
TSS (mg/L)	-	-	352±8
Chloride (Cl^-, mg/L)	-	0.7±1.9	39.4±5.4

Bicarbonate (HCO_3^-, mg/L)	-	18.4±3.5	102.4±3.5
Sulfate (SO_4^{2-}, mg/L)	-	1.6±0.8	28.3±4.7
Nitrate (NO_3^-, mg/L)	-	-	49±0.8
Phosphate (PO_4^{3-}, mg/L)	-	-	22.6±0.4
COD (mg/L)	-	-	166±13 (spiked with 10 mg/L TCL)
TCL (mg/L)	10 (spiked)	10 (spiked)	10 (spiked)

Table S8 Transformation products (TPs) of TCL identified from LC-MS (Source: Fig. S13).

Parent compound/TPs	**m/z**	**Structure**
TCL	444.47	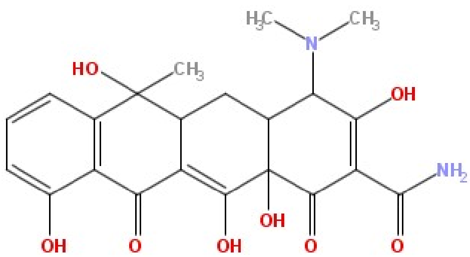
TP1	231.71	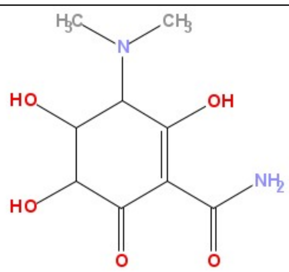
TP2	214.75	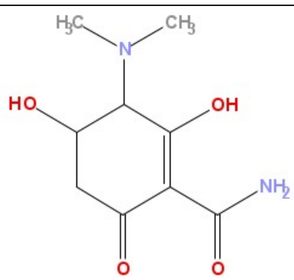
TP3	130.72	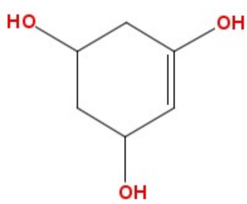

TP4	74.41	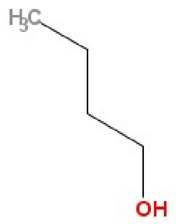
TP5	409.32	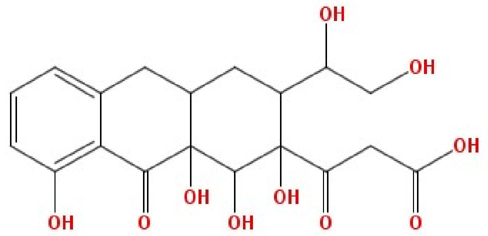
TP6	242.37	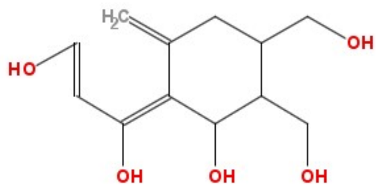
TP7	187.82	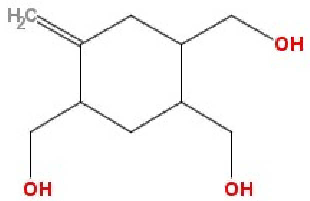
TP8	460.79	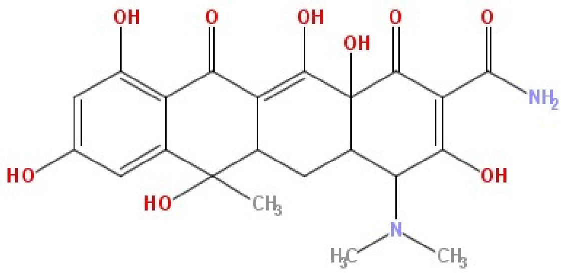
TP9	416.81	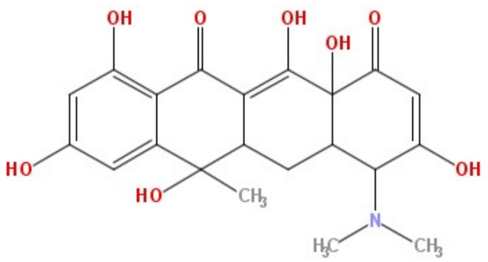

TP10	414.66	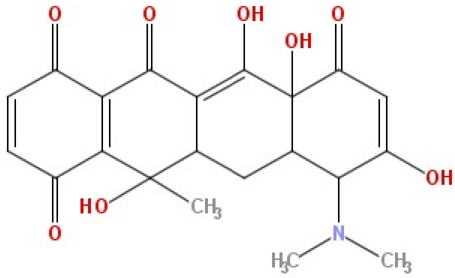
TP11	427.49	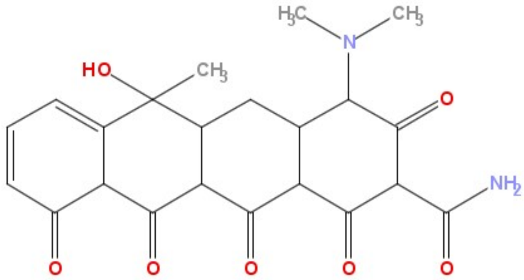
TP12	414.88	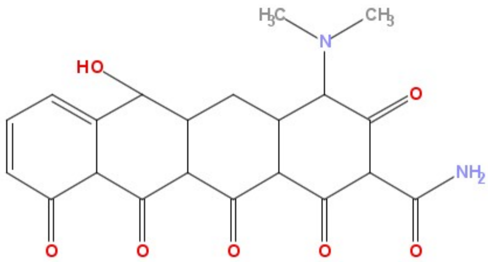
TP13	399.53	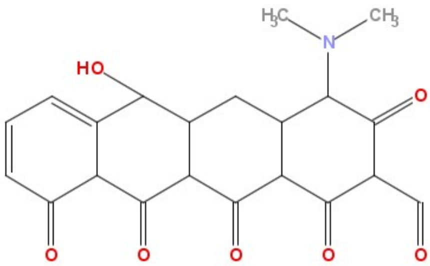
TP14	386.71	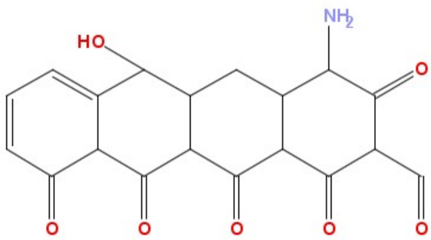

REFERENCES

1 M. Waqar, M. Imran, S. F. Adil, S. Noreen, S. Latif, M. Khan and M. R. H. Siddiqui, *Materials*, 2019, **13**, 35.

2 E. Vesali-Kermani, A. Habibi-Yangjeh, H. Diarmand-Khalilabad and S. Ghosh, *Journal of Colloid and Interface Science*, 2020, **563**, 81–91.

3 S. Vinoth, K. Subramani, W.-J. Ong, M. Sathish and A. Pandikumar, *Journal of Colloid and Interface Science*, 2021, **584**, 204–215.

4 S. R. Mishra, V. Gadore and M. Ahmaruzzaman, *International Journal of Environmental Analytical Chemistry*, 2023, 1–18.

5 D. Luo, P. Zhu, M. Duan, M. Liu, H. Lu and Z. Huang, *Separation and Purification Technology*, 2023, **311**, 123287.

6 S. Li, Y. He, F. Kong, W. Sun and J. Hu, *Water*, 2020, **12**, 2078.

7 J. F. Leal, V. I. Esteves and E. B. H. Santos, *Journal of Photochemistry and Photobiology A: Chemistry*, 2019, **372**, 218–225.

8 N. A. M. Saeed, E. Coetsee, R. E. Kroon, M. Bettinelli and H. C. Swart, *Optical Materials*, 2021, **119**, 111291.

9 P. Xiao, C. Shen, Y. Li, S. Cui, S. Chen and J. Yang, *Journal of the Taiwan Institute of Chemical Engineers*, 2024, **162**, 105611.

10 C. Pan, Z. Wang, Y. Lou, Y. Zhang, Y. Dong and Y. Zhu, *Journal of Materials Chemistry A*, 2021, **9**, 3616–3627.

11 Z. Yang, Q. Lin, G. Zeng, S. Zhao, G. Yan, M. B. M. Y. Ang, Y.-H. Chiao and S. Pu, *Journal of Membrane Science*, 2023, **669**, 121329.

12 M. Lathika Divya, Y.-S. Lee and V. Aravindan, *Physical Review Applied*, 2023, **19**, 034016.

13 V. Hasija, P. Singh, S. Thakur, V.-H. Nguyen, Q. Van Le, T. Ahamad, S. M. Alshehri, P. Raizada, B. M. Matsagar and K. C.-W. Wu, *Chemosphere*, 2023, **320**, 138015.

14 P. Ke, D. Zeng, J. Cui, X. Li and Y. Chen, *Catalysts*, 2022, **12**, 247.

15 E. Arulkumar and S. Thanikaikarasan, *Diamond and Related Materials*, 2024, **147**, 111294.

16 M. Momina and K. Ahmad, *International Journal of Biological Macromolecules*, 2024, **263**, 130253.

17 C. Wang, C. Yang, J. Qin, S. Rajendran and X. Zhang, *Materials Chemistry and Physics*, 2022, **275**, 125299.

18 Z. Zhao, X. Wang, Z. Shu, J. Zhou, T. Li, W. Wang and Y. Tan, *Applied Surface Science*, 2018, **455**, 591–598.

19 M. A. Cotarelo, F. Huerta, C. Quijada, J. M. Pérez, M. A. del Valle and J. L. Vázquez, *Journal of The Electrochemical Society*, 2006, **153**, A2071.

20 W. Shi, M. Li, X. Huang, H. Ren, F. Guo, Y. Tang and C. Lu, *Chemical Engineering Journal*, 2020, **394**, 125009.

21 X. Zou, B. Sun, L. Wang, H. Bai, X. Meng, C. Li and Z. Li, *Chemical Engineering Journal*, 2024, **482**, 148818.

22 H. Sun, C. Zou and W. Tang, *Colloids and Surfaces A: Physicochemical and Engineering Aspects*, 2022, **654**, 130105.

23 S. Wu, B. Yi and D. Lan, *Journal of Photochemistry and Photobiology A: Chemistry*, 2023, **444**, 115013.

24 Y. Qiu, J. Lu, Y. Yan, J. Niu and Y. Duan, *Surfaces and Interfaces*, 2022, **31**, 102009.

25 A. M. Asiri, A. Raza, M. K. Shahzad, M. M. Fadhali, S. B. Khan, K. A. Alamry, S. Y. Alfifi and H. M. Marwani, *Journal of Photochemistry and Photobiology A: Chemistry*, 2023, **438**, 114486.

26 U. Ghosh, A. Majumdar and A. Pal, *Materials Research Bulletin*, 2021, **133**, 111074.